# Lidar/IMU Integrated Navigation and Positioning Method

Zhigang Wang[1], Jiehua Liao[1], Hang Guo[1(✉)], and Min Yu[2(✉)]

[1] Nanchang University, Nanchang 330031, China
[2] Jiangxi Normal University, Nanchang 330021, China

**Abstract.** Aiming at the problem of large positioning accuracy of LiDAR odometry and mapping (LOAM) algorithm, this paper proposes a LOAM algorithm fusion Adaptive Particle Filter (APF) algorithm. Experiments show that the trajectory of the APF algorithm using the LOAM algorithm was half the accuracy of the trajectory using the LOAM algorithm. In order to better verify the accuracy effect, the R-fans 16-line laser radar was used to compare and analyze the test under closed and non-closed routes. The results show that under the closed route, the LOAM algorithm combines the APF algorithm to provide the accurate position trajectory for the car. In the non-closed route, due to the lack of closed-loop constraints, the motion distortion of the car is caused by the accumulation of errors. Through experiments, using the LOAM algorithm to merge the APF algorithm in the non-closed loop could also effectively compensate the motion distortion and filter out the noise, so as to achieve the effect of the trajectory correction, reduce the error with the real trajectory, and improve the positioning accuracy.

**Keywords:** R-fans 16-line lidar · Closed loop · Non-closed loop · LOAM algorithm · APF algorithm

## 1 Introduction

With the continuous rise of location-based service (LBS), indoor positioning has become an important direction [1, 2], and accurate positioning trajectories can greatly meet people's positioning needs. Experts at home and abroad have successively proposed improved proximity algorithm [3], dead reckoning algorithm [4], vision-based positioning algorithm [5] and multi-sensor fusion-based positioning algorithm [6–9]. The above method research is relatively deep and extensive, but all have certain limitations and defects. The limitation is that it only conducts positioning research for closed trajectories, and does not involve research on non-closed trajectories. The defect type is manifested in the inefficiency of the improved algorithm of the proximity method, the dead reckoning will cause drift, the vision-based positioning algorithm is too complex, and the positioning algorithm based on multi-sensor fusion is vulnerable to environmental factors. Therefore, the laser radar combined with the logistics trolley is used to form a laser radar trolley system [10], and the accuracy can be in the centimeter level. However,


W. Fu et al. (Eds.): ICMTEL 2021, LNICST 387, pp. 407–413, 2021.
https://doi.org/10.1007/978-3-030-82562-1_38

when solving the trajectory, the LOAM algorithm has no closed-loop constraints, which will produce motion distortion; at the same time, filtering and estimating the state of the variables at the current moment is an iterative process, and the points in the point cloud scanned by the radar are discretized. Ensure that the points of the previous frame of data are still scanned in the next frame. Therefore, an adaptive particle filter algorithm is used to optimize the position and attitude of the laser odometer to estimate the accuracy. The adaptive particle filter algorithm accelerates particle convergence, while taking into account the diversity of particles, using a smaller number of particles to obtain more accurate trajectory results. This paper combines the LOAM algorithm and the APF algorithm to correct the trajectory when calculating the trolley trajectory of closed and semi-closed routes, which can effectively improve the accuracy of trajectory positioning.

## 2 Principle of LOAM Algorithm

The essence of the LOAM algorithm is a laser odometer. The algorithm divides the SLAM problem into two algorithms that run simultaneously to realize real-time mapping. The main steps of the LOAM algorithm:

1. Extract feature points
2. Find the corresponding point of the feature point
3. Estimation of action

## 3 Definition of Particle Filter

Adaptive particle filter (APF) algorithm model: The state of the dynamic system is probably distributed to $p(x_0)$. The post-test probability distribution of the target state $x_k$ is $p(x_{0:k}|z_{1:k})$, $\{x_{0:k}^i, w_k^i\}_{i=1}^{N_s}$ is a particle population of the corresponding weight of $\{w_k^i, i = 0, \cdots, N_s\}$, where $x_{0:k} = \{x_j, j = 0, \cdots, k\}$ is the state set of 0 to k.

## 4 Fusion of LOAM Algorithm and APF Algorithm

### 4.1 The Initialization

Determine the movement coordinates of the trolley through the calibration of the position, for example, take the number of particles $N = 100$, filter the walking direction of the trolley, set the initial value of the weight to $1/N$, and according to the system setting, the sum of the weight of the particles is 1. Each particle represents the possible motion state of the trolley, that is, the possible position of the trolley.

### 4.2 State Transition of Particles

Taking into account the continuous transfer of particle states, the position of the trolley is constantly updated over time, and the Bayesian full probability formula is used to estimate its motion model.

$$P(X_{k,i}, X_{k+1,i+1}, U_{(k,k+1)}) \propto P(X_{0,0}|U_{i,0}) \prod_{k=1}^{i} P(X_k|X_{k+1}, U_k, U_{k+1}) \tag{1}$$

Where: $X_{k,i}$ represents the pose node of the $k$-the frame lidar at time $I$, $X_{k+1,i+1}$ represents the pose node of the $k$-the frame lidar at time $I$, and $U_{(k,k+1)}$ represents the transfer matrix between two adjacent frames of radar data obtained by the LOAM matching algorithm.

### 4.3 Particle Update

The APF algorithm approximates the true posterior probability of the system by continuously updating the position and weight of the particle. Through the motion model, the particle continuously updates the position, and at the same time updates the weight value by measuring the model particle.

The feature point screening and matching of the LOAM algorithm and the prior probability density function and posterior probability density function of the particles are combined to obtain an optimized fusion matrix function.

$$f(U) = \min f(\sum_{i=1}^{n} d_{\varepsilon i}(U) + \sum_{j=1}^{m} d_{Hj}(U)) \tag{2}$$

Where: $d_{\varepsilon i}$ is the distance between the i-th line characteristic point to line $\varepsilon$, $d_{Hj}$ is the distance between the j-th feature point to the surface $H$.

$d_{\varepsilon i}$ and $d_{Hj}$ are the distance from the $i$tch line feature point to the line and the $j$-the surface feature point to the surface respectively.

### 4.4 Re-sampling

The motion state and position of the trolley are estimated by selecting particles with larger weights. Using this distribution, the weight of the first particle:

$$\omega_t^{(i)} = \omega_{t-1}^{(i)} . \eta^{(i)}. \tag{3}$$

In the formula, the weight is selected by sampling method. If the particle set $\{ x_{0:k}^i \}_{i=1}^{N_s}$ can be obtained by the density function $q(x_{0:k}|z_{1:k})$, the weight is shown in the following formula:

$$w_k^i \propto \frac{p(x_{0:k}^i z_{1:k})}{q(x_{0:k}^i|z_{1:k})} \tag{4}$$

## 5 Experiment and Analysis

The experimental equipment uses R-fans16 cable and a laptop equipped with ubuntu system and ROS system. In order to compare the accuracy of positioning, the relevant paths were planned in advance. Four control points including the start point and the end point were set on the fully enclosed path and the semi-closed path respectively, and the precise control points were obtained by using a total station. The location under the coordinates, the experimental equipment is shown in Fig. 1, the experimental routes are respectively selected indoor fully enclosed routes and semi-enclosed routes.

**Fig. 1.** Experimental equipment diagram

### 5.1 Fully Enclosed Route Experiment

In a closed indoor environment, a stone is placed every other segment, and the trolley is slowly moving along the closed loop at a speed of 0.5 m/s. The MATLAB simulation results of the two closed-loop experimental trajectories are shown below (Figs. 2 and 3).

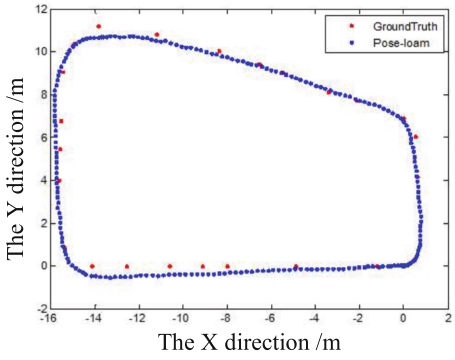


**Fig. 2.** Real trajectory and blue dot trajectory of LOAM algorithm

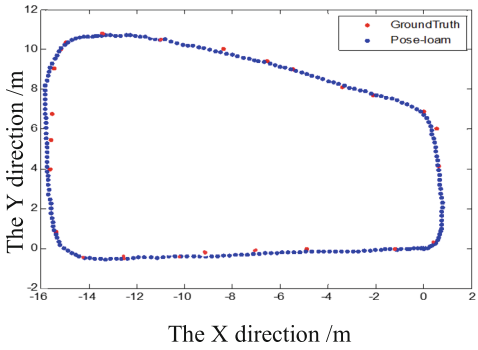


**Fig. 3.** Real trajectory and blue dot trajectory of LOAM-APF algorithm

**Table 1.** Trajectory positioning error of a fully enclosed route

| Direction error | LOAM | LOAM-APF |
|---|---|---|
| X direction error/m | 0.07 | 0.03 |
| Y direction error/m | 0.10 | 0.05 |

From Table 1, under the closed route, the positioning accuracy of LOAM-APF algorithm in the x direction is improved by 57.1%, and the positioning accuracy in the Y direction is improved by 50%.

### 5.2 Semi-closed Route Experiment

Four nodes are selected and a semi-enclosed route is planned. The trolley is slowly advancing at a speed of 500 mm/s. The MATLAB simulation results of the semi-circle experimental trajectory are shown in the figure below (Figs. 4, 5 and 6).

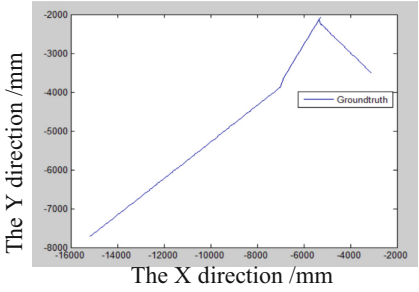


**Fig. 4.** Real trajectory

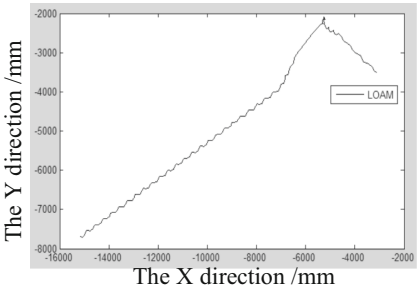


**Fig. 5.** Motion trajectory of LOAM algorithm

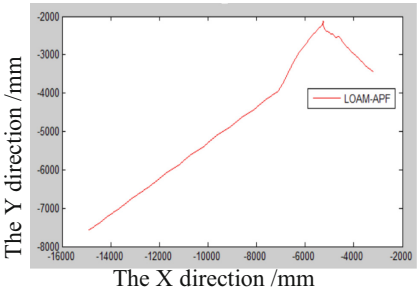


**Fig. 6.** Motion trajectory of LOAM-APF algorithm

**Table 2.** Trajectory positioning error of semi-closed route

| Error | LOAM | LOAM-APF |
|---|---|---|
| Positioning error/mm | 56 | 28 |
| Error respectively/% | 0.43 | 0.22 |

From Table 2, the standard deviation and positioning error distribution of using the LOAM-APF algorithm in the semi-closed route experiment are reduced by 50% compared to only using the LOAM algorithm, which greatly improves the accuracy of its positioning.

## 6 Conclusion

As the trajectory of the trolley increases, the trajectory calculated by the LOAM algorithm will fluctuate and deviate from the real trajectory, while the trajectory obtained by the LOAM-APF algorithm will basically not fluctuate. The LOAM-APF algorithm solves the problem of trajectory deviation in closed and semi-closed routes, which has certain practical significance.

**Acknowledgments.** The paper was supported by the projects of the National Natural Science Foundation of China (No. 41764002).

## References

1. Chen, X., Pang, J.: Protecting query privacy in location-based services. GeoInformatica **18**(1), 95–133 (2014)
2. Huang, B., Liu, J., Sun, W., et al.: A Robust indoor positioning method based on Bluetooth Low energy with Separate channel information. Sensors **19**(16), 3487 (2019)
3. Xu, H., Ding, Y., Li, P., et al.: An RFID indoor positioning algorithm based on Bayesian probability and K-nearest neighbor. Sensors **17**(8), 1806 (2017)
4. Sharp, I., Yu, K.: Sensor-based dead-reckoning for indoor positioning. Phys. Commun. **13**(PA), 4–16 (2014)
5. Yang, S., Ma, L., Jia, S., et al.: An improved vision-based indoor positioning method. IEEE Access **8**, 26941–26949 (2020)
6. Ma, M., Song, Q., Gu, Y., et al.: An adaptive zero velocity detection algorithm based on multi-sensor fusion for a pedestrian navigation system. Sensors **18**(10), 3261 (2018)
7. Shi, Y., Zhang, W., Yao, Z., et al.: Design of a hybrid indoor location system based on multi-sensor fusion for robot navigation. Sensors **18**(10), 3581 (2018)
8. Gao, Y., Wang, F., Li, J., et al.: Localization of mobile robot based on multi-sensor fusion. In: 2020 Chinese Control And Decision Conference (CCDC), pp. 4367–4372. IEEE (2020)
9. Li, H.X., Ao, L.H., Guo, H., et al.: Indoor multi-sensor fusion positioning based on federated filtering. Measurement **154**, 107506 (2020)
10. Karam, S., Lehtola, V., Vosselman, G.: Strategies to integrate IMU and LIDAR SLAM for indoor mapping. ISPRS Ann. Photogramm. Remote Sens. Spat. Inf. Sci. **1**, 223–230 (2020)